

DYNAMICAL CONSEQUENCES OF A STELLAR WIND IN HERBIG-HARO OBJECTS

R. D. SCHWARTZ¹

Physics Department, College of Arts and Sciences, University of Missouri, St. Louis

AND

M. A. DOPITA

Mount Stromlo and Siding Spring Observatories, Research School of Physical Sciences, Australian National University

Received 1979 July 19; accepted 1979 September 11

ABSTRACT

New spectrophotometric and radial-velocity data are presented for a number of southern Herbig-Haro objects. Combined with data obtained earlier on other objects, we have been able to show an inverse correlation between the modulus of the radial velocity and either the shock pressure or the degree of excitation of the shock. This is shown to be the result of acceleration of shocked cloudlets in a strong pre-main-sequence stellar wind. For the most energetic of the Herbig-Haro objects, stellar mass-loss rates in the range $10^{-6} \leq \dot{M} \leq 10^{-5} M_{\odot} \text{ yr}^{-1}$ are required to excite the nebulae.

Subject headings: shock waves — stars: emission-line — stars: mass loss — stars: pre-main-sequence

I. INTRODUCTION

The discovery of a number of new Herbig-Haro (H-H) objects at southern declinations (Schwartz 1977*a, b*) has added measurably to the original compilation by Herbig (1974). To gain a more detailed understanding of the physical nature of these objects, it is desirable to acquire systematic spectrophotometry and radial-velocity data. This serves both for comparative studies among the objects and to establish first-epoch data to determine whether the optical variability (Herbig 1969) is reflected in either radial-velocity variations or spectral variability, tentatively established in HH 2H (Böhm and Brugel 1979). Dopita (1978*a, b*) has reported spectrophotometric observations of a number of objects in Herbig's catalog accessible from the south, plus the southern objects HH 46, 47, and 101. In this paper we give radial-velocity and spectrophotometric data for a number of objects selected from the Schwartz (1977*b*) survey; and these and earlier results are used to establish evidence for a shocked cloudlet structure for H-H objects.

II. THE OBSERVATIONS AND RESULTS

The spectrophotometric measurements were made on the nights of 1978 April 1 and 2, using the 3.9 m Anglo-Australian Telescope (AAT). The Royal Greenwich Observatory Cassegrain spectrograph was used at the f/7.9 focus with its grating number 4, which gave complete spectrophotometry in the wavelength range 3500–7500 Å with a resolution close to 10 Å. The

detector was the AAT image photon-counting system (Boksenberg 1972; Boksenberg and Burgess 1973). The slit, $180'' \times 2''$, aligned E-W, was divided into six bins for data collection. Subsequent sky subtraction in the exposures, each of 900 s, was accomplished by removing a weighted mean of the five bins about the object from the bin containing the object. Flat field calibrations were made using a diffuse white-light source, and calibration of spectral sensitivity was made by observing Oke (1974) white-dwarf standards.

Photographic spectra were obtained in the interval 1977 March 21–23 with the Cassegrain spectrograph and Carnegie image tube attached to the 4 m telescope at Cerro Tololo Inter-American Observatory (CTIO). Radial-velocity measurements of the plates were carried out in the manner described by Schwartz (1978). The CTIO spectra cover the range 6000–7000 Å, and were obtained with a slit width of 200 μm and the 600 lines mm⁻¹ grating, yielding a dispersion of about 52 Å mm⁻¹ and a plate resolution of about 40 μm.

Results of the spectrophotometric observations are contained in Table 1. The ion and wavelength of emission are listed in the first two columns. In successive columns are listed the relative intensities $I(\lambda)$ uncorrected for reddening, and the relative fluxes $F(\lambda)$ corrected for reddening, for each of six H-H objects. Two methods have been used to estimate the reddening for each of six H-H objects. The first method employs the observed Balmer decrement to determine the amount by which the relative intensities must be de-reddened to obtain a fit to the case B recombination spectrum of hydrogen. The logarithmic reddening constant at Hβ from the fits for each object are listed in the first row following the intensities in Table 1 as C_{Bal} . Dopita (1978*b*) has also shown that

¹ Visiting Astronomer, Cerro Tololo Inter-American Observatory, supported by the National Science Foundation under contract AST 74-04128.

TABLE 1
SPECTROPHOTOMETRIC DATA ON SOUTHERN H-H OBJECTS

Ion	λ	HH 49		HH 50		HH 54B		HH 54C		HH 56		HH 57	
		I(λ)	F(λ)										
[O II]	3727,29	192.8	283	97.6	198	148	332	174	505	180	328	185	433
H δ	3889	(10)	(13)	-	-	-	-	-	-	10.0	16.5	-	-
Ca II	3934	-	-	-	-	-	-	-	-	10.5	16.9	-	-
He, Ca II	3967-70	9.5	12.8	-	-	-	-	-	-	19.0	29.9	-	-
[Ne III]													
[S II]	4068,76	16.3	21.1	<7	<11	18.3	31.3	22.0	45	44.8	66.9	<36	
H δ	4101	13.0	16.7	10	15.8	18.0	30.3	10	19.8	12.0	17.6	-	-
H γ	4340	33.5	39.8	30	40.8	32.0	45.6	23	36.6	28.9	38.0	-	-
[Fe III], [O III]	4363	≥ 4	≥ 5	-	-	-	-	-	-	≥ 2	≥ 3	-	-
Mg I	4562,71	-	-	-	-	-	-	-	-	12.0	13.9	-	-
H β	4861	100 \pm 4		100 \pm 7		100 \pm 9		100 \pm 11		100 \pm 3		100 \pm 16	
[O III]	4959	16.3	15.8	-	-	-	-	-	-	20.7	19.9	-	-
[O III]	5007	66.3	63.7	9.7	9.0	>9	>8	41.5	37	49.2	46.2	-	-
[Fe II]	5158	(9)	(8)	-	-	28.6	23.8	36	28	20.2	17.7	-	-
[NI]	5199	-	-	-	-	56.5	45.9	105	80	53.9	46.2	61	49
[Fe II]	5261,73	-	-	-	-	15.6	12.2	-	-	11.2	9.3	-	-
[N II]	5754	-	-	-	-	-	-	-	-	14.6	9.9	-	-
He I	5875	-	-	-	-	-	-	-	-	12.1	7.9	-	-
[O I]	6300	43.2	29.6	80.8	40.9	459.7	210.7	587	210	356	199	328	143
[O I]	6363	8.5	5.8	27.9	13.8	128.3	57.4	180.8	91	99.6	53.2	118	51
[N II]	6548	30	19.7	34	15.8	88	36.6	160	51	70	36.7	61	24
H α	6563	373	243	526	242	726.5	299.3	972	302	552	286	744	290
[N II]	6584	82.4	53.6	122	55.6	350	143.0	398	122	210	108	225	87
[S II]	6717	34.8	22.1	131	57.2	366.3	142.3	616	177	259	128	328	120
[S II]	6731	42.4	26.9	127	55.2	370.6	143.2	558	159	315	156	356	130
[Fe II]	7155	-	-	-	-	51.4	17.2	89	21	24	10.7	-	-
[Ca II]	7291	-	-	-	-	133.1	42.5	213	47	45	19.3	-	-
[O II]	7324												
[Ca II]	7330	36	21	89	32	146.2	46.3	197	43	51	21.7	-	-
C_{Bal}		0.56 \pm .25		1.02 \pm .28		1.16 \pm .13		1.66 \pm .3		1.00 \pm .18		1.23	
$C_{[\text{S II}]}$		0.0		>1.0		1.10		1.26		0.43		>0.55	
* C_{adopted}		0.56		1.02		1.14		1.52		0.86		1.23	
sec Z		1.58		1.66		1.50		1.47		1.02		1.03	
v_s (km s $^{-1}$)		No fit		62		≤ 60		66-76		65-73		≤ 60	
n_1		~ 100		40		≥ 40		15-20		67-91		≥ 65	

*Heaviest weight has been given to the C_{Bal} values in computing C_{adopted} owing to uncertainties in the [S II] intensities and the model-dependent nature of $C_{[\text{S II}]}$.

the violet and red lines of [S II] can be used in the context of shock-wave theory to estimate the reddening parameter, and these results are listed as $C_{[\text{S II}]}$ in Table 1. The reddening parameter adopted for the correction of the fluxes is listed as C_{adopted} . Also noted is the air mass (sec z) at which each of the objects was observed. Since a relatively narrow slit was used, and since guiding was accomplished with a red-sensitive television camera, the relative intensities of lines in the violet portion of the spectrum could suffer underestimation owing to atmospheric dispersion, especially where sec $z \gtrsim 1.5$. At the bottom of Table 1 we list the results of fits of the relative line intensities of [O III]/[O I], [O III]/[O II], and [S II] ratios using shock-wave models which yield the shock velocity (v_s) and the preshock density (n_1) (Dopita 1977). Since these calculations assume complete pre-ionization of the gas entering the shock, and since there is strong evidence that a large proportion of the preshock gas is neutral (Dopita 1978b; Schwartz 1978), the velocities

listed are probably lower limits to the true shock velocities.

In Table 2 we list the results of the heliocentric radial-velocity measurements. Measurements were made on the red lines of [O I], [N II], H α , and [S II]; and the table lists the mean and standard deviation obtained for each object from these lines. The internal probable error is estimated to be about 10 km s $^{-1}$, indicating that the greater uncertainties associated with some of the objects probably result from the difficulty of locating line centers in untraced spectra which exhibit structure perpendicular to the dispersion.

The radial-velocity structure associated with HH 47 is complex. The emission lines exhibit a "tilt" indicating a velocity range of -108 to -129 km s $^{-1}$ from the NE to the SW portion of the object, a distance of 5". Moreover, a "bridge" of nebulous material appears to connect HH 47 with HH 46, which is embedded in a small dark cloud (see Schwartz 1977a; Dopita 1978a). The "bridge" appears to extend

TABLE 2
HELIOCENTRIC RADIAL VELOCITIES FOR HERBIG-HARO OBJECTS

Object	V_r (km s $^{-1}$)	Object	V_r (km s $^{-1}$)
HH 47.....	-121 ± 10	HH 54E.....	-67 ± 5
HH 49.....	$+25 \pm 3$	HH 54F.....	-32 ± 7
HH 50.....	$+30 \pm 5$	HH 54G.....	-78 ± 6
HH 52.....	-99 ± 10	HH 56.....	$+36 \pm 5$
HH 53.....	-101 ± 23	HH 101N.....	-89 ± 14
HH 54B....	-41 ± 4	HH 101S.....	-51 ± 9

about 35" from HH 47 to the rim of the dark cloud in the [S II] lines. The [S II] lines in the bridge are each split, one with a velocity component of about -150 km s $^{-1}$, and one with a component of about 5 km s $^{-1}$ (probably representing background [S II] emission from the surrounding Gum nebula). The extraordinary low-excitation character of HH 47 has been pointed out in Dopita's (1978a) study.

Among the other objects studied here, the object HH 54D appears to be a star with continuum only. It is not clear whether the star is physically related to the several H-H knots in HH 54. Knots 54F and 54G were not identified in the Schwartz (1977b) survey. Both lie in position angle 288° from 54B; 54F is about 5" from 54B, and 54G is about 19" from 54B.

III. DISCUSSION

Among the H-H objects studied to date, two southern objects appear to exhibit the greatest excitation extremes. First, HH 47 possesses a remarkably low-excitation state, dominated by lines of [N I], [O I], [S II], [Fe II], and the Balmer lines (see Dopita 1978a, b). Second, HH 49 in the Cha T1 association exhibits the smallest intensities in the [O I] and [S II] lines of any H-H objects known, with a relatively high [O III]/H β ratio, suggesting a higher excitation state than any other H-H object (although HH 2H and 2G have comparable [O III]/H β ratios).

Although most H-H objects exhibit spectra which can be accounted for by the shock-wave models (Dopita 1978b), HH 47 and HH 49 cannot be well matched by the plane shock calculations. Dopita suggests that HH 47 may be in a nonequilibrium state, in the sense that a constant shock velocity and preshock density may not be maintained for a time comparable to the recombination time in the postshock gas. Thus, the nebula is probably a rapidly cooling knot with decreasing (or no) energy input. HH 49, on the other hand, has a spectrum more reminiscent of that produced by photoionization. This may be the case, but an alternative explanation is that the shock is so young that recombination in the postshock gas is only just beginning. The presence of [O I] appears to favor the latter viewpoint.

We also note in the present data that three of the 12 H-H nebulae measured indicate positive radial velocities. Thus, the statistics are not greatly different from those of the northern hemisphere in which about 75% of the objects exhibit negative radial velocities.

The conventional interpretation of this phenomenon is that the shocks driven out of a pre-main-sequence star embedded in a dark cloud will preferentially be seen upon emergence at or near the front side of the cloud, thus yielding a negative line-of-sight velocity. Shocks propagating in the opposite direction (especially directly opposite the star) will tend to be obscured by the dark cloud.

Dopita (1978b) proposed a model complex of H-H objects, such as HH 2 or HH 24, in which a massive protostar drives out by virtue of its mass-loss or radiation pressure an optically thick dust shell which acts as a piston on the circumstellar medium, driving a shock into the stationary material before it. Rayleigh-Taylor instabilities and clumpiness in the circumstellar medium cause severe departures from sphericity. On the other hand, Schwartz (1978) believes that a strong mass outflow from the pre-main-sequence object can sweep out a cavity around the star to a considerable fraction of a parsec and that negligible emission comes from the weak outer transition shock. In this second interpretation the H-H objects are presumed to represent radiating bow shocks moving into dense cloudlets caught deep in this stellar-wind flow. Sustained pressure from the stellar wind could eventually accelerate the cloudlets, giving radial velocities comparable with those observed. This situation bears close analogies to that proposed by McKee and Ostriker (1977) for supernova remnants.

This latter model enables one to understand certain spectral peculiarities of H-H objects, not explicable by an assumption of plane-parallel geometry. Schwartz (1978) suggested that the bow shock will involve a greater proportion of neutral postshock gas than a plane shock with the same geometrical cross section and flow parameters. Thus, low excitation lines of [O I] and [N I] would be enhanced (as in HH 47; see Dopita 1978a) and the increased ratio of collisional excitation to collisional ionization of hydrogen will give a steeper Balmer decrement. It is interesting to note that the reddening obtained from [S II] line ratios here and by Dopita (1978b) is generally less than that obtained from the Balmer decrement (assuming pure recombination cascade), which suggests the presence of collisional effects.

Radial-velocity data can give a very simple way of distinguishing between the two contending models. In the case of a shock moving into stationary circumstellar material, the observed radial velocity with respect to the cloud can never be greater than the shock velocity. So, since the degree of excitation is dependent on the shock velocity, shocks with both low excitation and high velocity are impossible. In the case of an accelerated cloudlet, on the other hand, the situation is more complex. When a cloudlet is first engulfed by a stellar wind, two distinct shocks are formed, a stand-off bow shock and a cloudlet shock driven by the effective surface pressure on the cloudlet, which can exceed the intercloud ram-pressure value by an appreciable (2-5) factor. Since the density in the stellar wind is lower than in the cloudlet,

the bow-shock velocity is appreciably higher than the cloudlet shock. Thus, the cooling time in the former is much longer than in the latter; so at early times the optical emission is dominated by the relatively slow-moving cloudlet shock. Later on, the situation can be reversed, since after the shock has moved through the cloudlet, the slowly cooling disklike cloudlet, "crushed," in the words of McKee and Ostriker (1977), is accelerated toward the velocity of the stellar wind. The optical emission, then, is dominated by the bow shock of ever-decreasing shock velocity and by recombining gas in the postcloudlet shock gas. The latter component is necessary to explain the strengths of the [O I] and [N I] lines and the Balmer decrement in the low-excitation shocks (Dopita 1978*b*; Schwartz 1978). The sense of evolution of the optical emission in the cloudlet model is therefore from relatively high-excitation, low space velocity shocks to low-excitation emission in a rapidly moving cloudlet.

The shock-wave theory developed by Dopita (1978*b*) has shown that measurement of the red [S II] ratio $\lambda 6731/\lambda 6717$ alone is sufficient to give the pressure driving the shock, provided that the pressure terms due to magnetic field are negligible. The density given by the [S II] ratio $N_{[\text{S II}]}$ is related to the shock velocity V_s and preshock density n_1 by

$$N_{[\text{S II}]} = (43 \pm 15) \left(\frac{V_s}{100 \text{ km s}^{-1}} \right)^2 \left(\frac{n_1}{\text{cm}^3} \right), \quad (3.1)$$

that is to say, the density of the S^+ zone is proportional to the ram pressure.

Figure 1 gives the relationship between the pressure found in this manner and the modulus of the heliocentric radial velocity, where points have been derived from this work, from the references already cited, from Strom, Grasdalen, and Strom (1974), and from unpublished results of Schwartz. No attempt has been made to correct the radial velocities for galactic rotation, but this should be unimportant, since the errors of measurement are at least as great as this effect, and the distances of some of the dark clouds are not known accurately. A typical error on $|V_r|$ will be $20\text{--}30 \text{ km s}^{-1}$. It is remarkable that no H-H shock driven by a high pressure has high radial velocity, whereas a substantial fraction of those driven at low pressure have high velocities. Such a result might have come about if the preshock density in the high-pressure shocks was great enough to produce a slower shock despite the higher pressure. This supposition is not borne out by observation, as is apparent from Figure 2. Here, the modulus of the heliocentric radial velocity is plotted against an excitation parameter $\log [I(6300)/I(5007)]$. An approximate calibration of this parameter with the shock velocity from the computations by Dopita (1977) is also given in this Figure. High-excitation objects tend to have the lowest radial velocities, while many of the low-excitation objects have radial velocities greater than the velocity of the shock which is propagating through them. This is impossible if the preshock material is stationary. Only a model involving

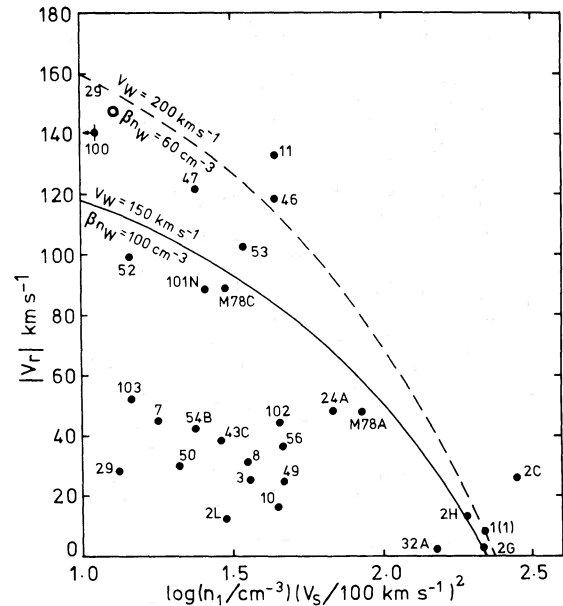


FIG. 1.—The modulus of the heliocentric radial velocity against the shock pressures for H-H objects. The curves are theoretical curves for various stellar-wind parameters, assuming that H-H objects are shocked cloudlets accelerated by this wind. The points for HH 52 and 53 are computed from poorly calibrated spectra, not presented here. The open circle for HH 29 is the fully corrected space motion using the proper-motion measurement of Cudworth and Herbig (1979).

the interaction of a cloudlet and a strong stellar wind is capable of explaining these relationships. The low-excitation, low-driving-pressure shocks would be a natural consequence of a strong stellar wind encountering a cloudlet which already possesses a

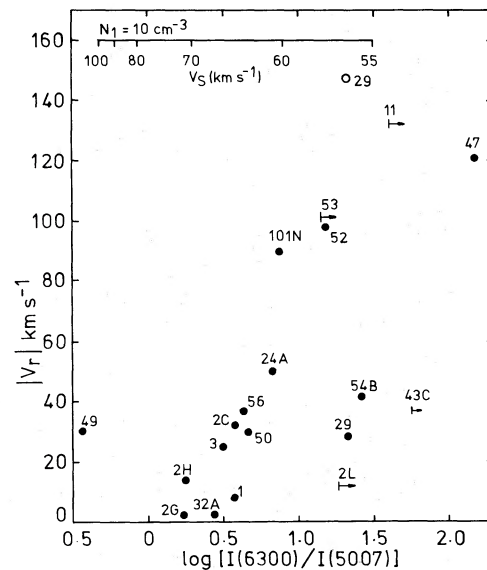


FIG. 2.—The modulus of the heliocentric radial velocity against a shock excitation parameter. The approximate calibration of this parameter with shock velocity is shown on the upper edge of the figure. Objects with high space velocities tend to have low shock velocities.

substantial space velocity in the direction of the stellar wind. This velocity is presumably acquired from the past combined effects of the stellar-wind ram pressure, so objects of this type are older and/or of lower mass per unit area. At the opposite extreme, a cloulet which is virtually stationary with respect to the stellar wind will suffer a much higher surface pressure, which will drive a higher excitation shock into it.

On the basis of this cloulet shock model, Figure 1 can be used to estimate the mean parameters of the stellar wind. If V_w is the velocity and n_w the density of the stellar wind, then (McKee and Cowie 1975)

$$n_1 V_s^2 = \frac{\gamma_c + 1}{\gamma + 1} \beta n_w V_w^2, \quad (3.2)$$

where

$$\beta = 3.15 - 4.78x + 2.63x^2,$$

$$x = \frac{\gamma + 1}{\gamma_c + 1} \frac{V_s}{V_w},$$

and γ_c and γ are the ratios of specific heats of the cloulet material and the stellar-wind material, respectively. The factor β arises because the surface pressure on the cloud is enhanced over the intercloud value. If the cloud has a systemic velocity V_c in the direction of the stellar wind, then V_w should be replaced by $(V_w - V_c)$ in equation (3.2). In Figure 1 we have plotted curves derived from equation (3.2) on the assumption that $\gamma = \gamma_c$ and that the maximum ram pressure is defined by the group of points formed by HH 1, 2, and 32. Since geometrical projection effects constrain $|V_r|$ to be less than V_c , these curves should (and do) define an approximate upper envelope to the observed values; indeed, the $V_w = 200 \text{ km s}^{-1}$ curve passes close to the space-motion-corrected point for HH 29, using the proper motion of 145 km s^{-1} measured by Cudworth and Herbig (1979).

A second effect, not taken into account, is that the wind density must fall approximately quadratically as the distance from the star. Cloulets, whose mass-per-unit area normal to the wind is too great, will not be efficiently accelerated but will move more slowly to regions of lower stellar-wind density, and this too will force them to fall below the envelope curve.

The importance of these effects is illustrated by the way points from different H-H knots in the same complex distribute themselves in Figure 1. In HH 2 for example, the bright knots 2C, 2G, and 2H gather in the high-pressure, low-velocity region; however, HH 2L, a faint knot a long way out, has low pressure and excitation (as expected from the geometrical dilution of the stellar wind) but also has a low velocity. HH 2 is therefore either young or contains massive cloulets, so that cloulet acceleration has been negligible. HH 46 and 47, on the other hand, are very well accelerated cloulets with low pressure and low excitation and represent the other end of the evolutionary sequence. HH 47 has the lowest pressure, as befits its position farthest from the central star. The

complex HH 7, 8, 10, and 11 is interesting. The ram pressures are ordered according to decreasing distances from the central star (an infrared source found by Strom, Grasdalen, and Strom, 1974). HH 7, 8, and 10 have intermediate radial velocities, but HH 11, although only marginally closer to the star than HH 10, lies very close to the upper envelope of velocity. Presumably HH 11 is a cloulet of lower surface mass than HH 7, 8, or 10.

It should be noted that the theoretical curves plotted in Figure 1 depend upon the assumption that the cloulet shock is responsible for the observed luminosity of an H-H nebula. The results suggest mean stellar-wind parameters of $V_w - V_c = 200 \text{ km s}^{-1}$ and $\beta n_w = 60 \text{ cm}^{-3}$, where V_c is the cloulet velocity in the direction of the stellar wind. Since Figure 2 and the more detailed shock modelling of Dopita (1978b) suggest that the radiating shocks have $50 \leq V_s \leq 80 \text{ km s}^{-1}$, equation (3.2) gives $1.2 \leq \beta \leq 2.1$. We, hence, adopt a mean value of $n_w = 35 \text{ cm}^{-3}$. For an isothermal shock, the cloulet shock velocity V_s is $(V_w - V_c)[1 + (n_1/n_w)^{1/2}]^{-1}$ (McKee and Cowie 1975), so the mean preshock cloulet density would be $n_1 \approx 150 \text{ cm}^{-3}$.

Another alternative is that the bow shock might dominate the observed luminosity, in which case the radiating shock velocity will be $V_w - V_c$, and the ram pressure on the cloulet (eq. 3.2) may not be sufficient to produce a luminous cloulet shock. In the model suggested by Schwartz (1978), the luminous bow shocks require, typically, $n_w = 200 \text{ cm}^{-3}$ and $V_w - V_c = 80 \text{ km s}^{-1}$, parameters which also satisfy the observed conditions. As indicated in the discussion above, it is indeed possible that a cloulet shock would dominate in the initial encounter with the stellar wind, and as the cloulet accelerates, the bow shock would become dominant as the source of the low-excitation spectrum. At intermediate stages in the acceleration, the cloulet shock might dominate in the lines of [O I], [N I], etc., while the bow shock would produce the higher excitation lines of [O III], [N II], etc. An important constraint on the cloulet-shock alternative is that for $V_w - V_c \geq 100 \text{ km s}^{-1}$, the bow-shock temperature will exceed 10^5 K . A detailed shock-wave calculation using the bow-shock/cloulet-shock geometry will be required to assess the relative importance of each shock as a function of $V_w - V_c$, and to determine the degree to which one might expect a high-temperature bow shock to contribute to the total observed luminosity of the system.

The energy requirements of the stellar-wind source can be estimated if the distance of the cloulet from the star is known. Cohen and Schwartz (1979) have recently identified a 17th mag T Tauri star 25" (0.06 pc) SE of HH 1 as the probable exciting source for that nebula. Using the mean stellar-wind parameters suggested above, and assuming that the H-H nebula (cloulet) presents a circular cross section with radius 3" (1500 AU) to the wind, the kinetic energy in the cross-sectional flow is $0.13 L_\odot$. Böhm, Siegmund, and Schwartz (1976) have measured the total optical luminosity in HH 1 to be about $0.07 L_\odot$. Thus, the

wind has sufficient energy to produce the observed luminosity, although the efficiency factor (~ 0.5) with which this occurs may be a bit high, since one also expects considerable energy to be deposited in other forms (e.g., in the cloulet acceleration). If the wind flow from the star is isotropic, one requires $\dot{M} \approx 10^{-5} M_{\odot} \text{ yr}^{-1}$, a figure which may be prohibitively high, since it equals or exceeds the optical and infrared output from the star. The situation is alleviated if one assumes an anisotropic equatorial flow which expands to the cross section of HH 1, requiring $\dot{M} \approx 10^{-6} M_{\odot} \text{ yr}^{-1}$ ($3.6 L_{\odot}$) of wind.

In the few cases where optical candidates exist for the exciting stars of H-H nebulae, the stars are T Tauri stars (Schwartz 1975; Cohen and Schwartz 1979). Also, the infrared energy distributions of IR sources apparently associated with some H-H nebulae are compatible with T Tauri stars (Strom, Grasdalen, and Strom 1974). At the same time, one cannot eliminate the possibility that such stellar-wind flows might be associated with earlier-type stars, such as embedded Herbig Ae/Be stars, in some cases.

Garrison (1978) finds outflow velocities of 70–210 km s^{-1} and mass-loss rates of 5×10^{-8} to $9 \times 10^{-6} M_{\odot} \text{ yr}^{-1}$, using measurements of the Balmer excess and the $\text{H}\alpha$ line profile (Garrison and Anderson 1977). Kuan and Kuhl (1975) find, from analysis of the $\text{H}\beta$ and $\text{H}\gamma$ profiles, velocities of 240–550 km s^{-1} and mass-loss rates of 6×10^{-8} to $0.5 \times 10^{-6} M_{\odot} \text{ yr}^{-1}$. In any case, especially for the cooler T Tauri stars, one requires an extremely efficient mechanism to produce a substantial fraction ($\geq 10\%$) of the total stellar luminosity in the form of a wind. DeCampli (1979) has recently reported theoretical explorations which indicate that rotational kinetic energy of the star can, in fact, be efficiently converted to a stellar wind.

We wish to thank the Telescope Allocation Committee for providing AAT observing time. Likewise, we express our gratitude to the Director and staff of CTIO. One of us (R. D. S.) was supported in part by a Faculty Research grant from the University of Missouri, St. Louis, and in part by NSF grant AST 7902787.

REFERENCES

- Böhm, K.-H., and Brugel, E. W. 1979, *Astr. Ap.*, **74**, 297.
 Böhm, K.-H., Siegmund, W., and Schwartz, R. D. 1976, *Ap. J.*, **203**, 399.
 Boksenberg, A. 1972, *Proc. ESO/CERN Conf. Auxiliary Instrumentation for Large Telescopes*, Geneva, May 2–5, p. 295.
 Boksenberg, A., and Burgess, D. E. 1973, *Proc. Symp. Astronomical Observations with Television-Type Sensors*, Vancouver, May 15–17, p. 21.
 Cohen, M., and Schwartz, R. D. 1979, *Ap. J. (Letters)*, **233**, L77.
 Cudworth, K. M., and Herbig, G. 1979, *A.J.*, **84**, 548.
 DeCampli, W. 1979, *Astrophysics Workshop on Star Formation*, Santa Cruz, July 15–August 3.
 Dopita, M. A. 1977, *Ap. J. Suppl.*, **33**, 437.
 ———. 1978a, *Astr. Ap.*, **63**, 237.
 ———. 1978b, *Ap. J. Suppl.*, **37**, 117.
 Garrison, L. M., Jr. 1978, *Ap. J.*, **224**, 535.
 Garrison, L. M., Jr., and Anderson, C. M. 1977, *Ap. J.*, **218**, 438.
 Herbig, G. H. 1969, in *Non-Periodic Phenomena in Variable Stars*, ed. L. Detre (Dordrecht: Reidel), p. 75.
 ———. 1974, *Lick Obs. Bull.*, No. 658.
 Kuan, P., and Kuhl, L. V. 1975, *Ap. J.*, **199**, 148.
 McKee, C. F., and Cowie, L. L. 1975, *Ap. J.*, **195**, 715.
 McKee, C. F., and Ostriker, J. P. 1977, *Ap. J.*, **218**, 148.
 Oke, J. B. 1974, *Ap. J. Suppl.*, **27**, 21.
 Schwartz, R. D. 1975, *Ap. J.*, **195**, 631.
 ———. 1977a, *Ap. J. (Letters)*, **212**, L25.
 ———. 1977b, *Ap. J. Suppl.*, **35**, 161.
 ———. 1978, *Ap. J.*, **223**, 884.
 Strom, S. E., Grasdalen, G. L., and Strom, K. M. 1974, *Ap. J.*, **191**, 111.

M. A. DOPITA: Mount Stromlo and Siding Spring Observatories, Private Bag, Woden. P.O. ACT 2606, Australia

R. D. SCHWARTZ: Department of Physics, University of Missouri, 8001 Natural Bridge Road, St. Louis, MO 63121